African Corrosion Journal
Official publication of the Corrosion Institute of Southern Africa
www.africorr.org.za

Effect of ruthenium laser cladding on metal dusting of 304L stainless steel

Yonela A Mgwebi [1,a,*] & Josias W van der Merwe [1,b]

[a] aziwe92@gmail.com, [b] josias.vandermerwe@wits.ac.za

1 School of Chemical and Metallurgical Engineering, University of the Witwatersrand, Johannesburg, Wits 2050, South Africa, DST/NRF Centre of Excellence in Strong Materials.

ARTICLE INFO

Keywords: laser cladding, uniform oxide layer, ruthenium

ABSTRACT

Metal dusting is a catastrophic form of carburization which occurs in carbon supersaturated environments in the temperature range of 400-800ºC. Industries often plagued by metal dusting include the petrochemical, direct iron ore reduction and steam reforming industries. This phenomenon can cause significant damage to processing units, causing major financial losses as a result of high maintenance costs and shutdowns. Most materials suffer from metal dusting degradation. In an attempt to mitigate metal dusting of 304L stainless steel, 304L samples were laser cladded with ruthenium and stainless steel powders where ruthenium compositions of 0wt%, 0.5wt%, 2wt%, 5wt% and 10wt% were investigated. Prior to exposure the samples were ground to a surface finish of 500 grit paper. Toluene was used as the carbon gas and entered the furnace at a temperature of 60ºC, with a flowrate of 100 mL/min. The tests were performed at an operating temperature of 750ºC over 96 hours. SEM and EDS surface analyses showed that after 24 hours exposure, all the samples formed a uniform oxide layer. There was no evidence of pits on the surface of the samples. The Raman spectroscopy results showed that all the surfaces were covered with amorphous carbon with no spinel. However after 72 hours exposure, a thick layer of coke was identified on the 0wt%, 0.5wt% and 2wt% ruthenium samples, these samples also had oxide layers with defects. However, these oxide defects were able to self-heal. The 5 and 10wt% ruthenium samples performed much better because they formed and retained a continuous and non-defective oxide layer.

1 Introduction

Austenitic stainless are one of the most preferred groups of alloys for high temperature applications, due to their high creep resistance, superior mechanical properties as well as their ability to form a protective oxide against corrosion attack under such conditions (Rowlands 2006; Zhang et al. 2012). Metal dusting, which is a high temperature corrosion process and is defined as catastrophic carburization attack, often attacks stainless steels once the protective oxide is defective or has failed (Strauβ et al. 1999; Grabke et al. 2003; Zhang & Young 2007; Chun & Ramanarayanan 2007; Geers et al. 2013). Studies (Szákalos et al. 2002a; Szákalos et al. 2002b; Szákalos 2003) have shown that metal dusting occurs by catalytic deposition of carbon onto the metal substrate and the carbon subsequently dissolves in the substrate, forming carbides. These carbides dissolve when they are oxidised, resulting in an austenitic surface free of carbides. A graphite sub-structure channel is formed on the austenitic surface and enhances the formation of chromium and iron oxides. The formation of graphite causes volume expansion of the austenitic phase, which results in the disintegration of the austenitic surface into small metallic particles (Szákalos 2003; Szákalos 2004; Zhang et al. 2012). The control of metal dusting can best be achieved by preventing the dissolution of carbon into the metal substrate, by the addition of an inhibitor such as H_2S or PH_3 which inhibits the dissolution of carbon into the substrate by occupying the carbon gas entry sites (Palasantzas et al. 2004; Agüero et al. 2011). Secondly, a surface barrier which prevents carbon dissolution is needed and this can be in the form of a dense, adherent and continuous oxide layer. The oxide layer is the most possible solution, because austenitic steels are designed in order to form this protective oxide layer. The oxide layer slows down carbon transport to the matrix because it has low solubility of carbon (Zeng et al. 2002; Zeng & Natesan 2006).

Many studies (Lin et al. 2004; Zhang & Young 2007; Melo-Máximo et al. 2013) have been conducted in an attempt to protect 304L against metal dusting and have shown promising results. This work endeavors to control metal dusting by laser cladding varied ruthenium concentrations onto a 304L substrate.

2 Experimental Procedure

The samples were laser cladded with ruthenium and stainless steel powders where the ruthenium compositions investigated were 0wt%, 0.5wt%, 2wt%, 5wt% and 10wt%. Prior to exposure the samples were ground to a surface finish of 500 grit paper. Toluene was used as the carbon gas source which entered the furnace at a temperature of 60ºC, with a flowrate of 100 mL/min. The tests were performed over a period of 24 and an additional 72 hours, at an operating temperature of 750ºC. After exposure, the samples underwent surface analysis using a ΣIGMA, CARL ZEISS SEM, using the secondary detector and backscattered modes; and Raman spectroscopy using the Horiba Jobin-Yvon LabRAM HR Raman spectrometer with an excitation wavelength of 514.5 nm. The exposed samples were sectioned along the cross-section and then metallographically prepared, where they were polished to a one micron finish for analysis of the cross-section. Cross-sectional analysis was conducted using the SEM, as well to evaluate for any cracks or defects formed in the material as a result of metal dusting.

3 Results

The cross-sectional microstructure analysis prior to exposure showed that the laser cladded surface layer had a finer grained microstructure compared to the 304L substrate, Figure 1. This is in agreement with what Lekala *et al.* and Olubambi *et al.* found; laser cladding on its own results in a fine microstructure with a high density of grain boundaries and the addition of ruthenium has the same result (Olubambi et al. 2009; Lekala et al. 2012).

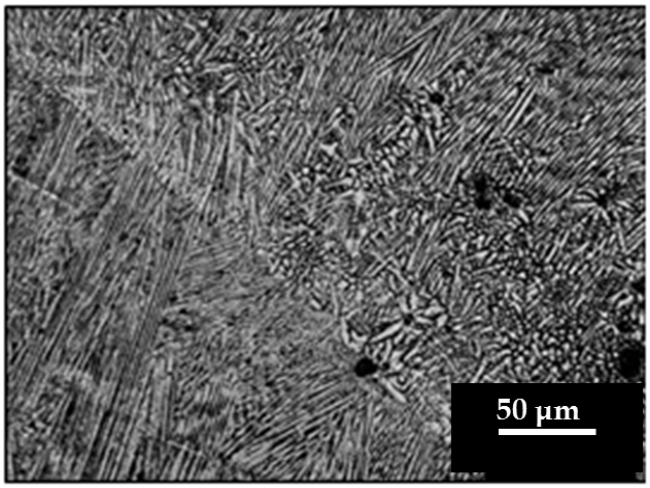

(a)

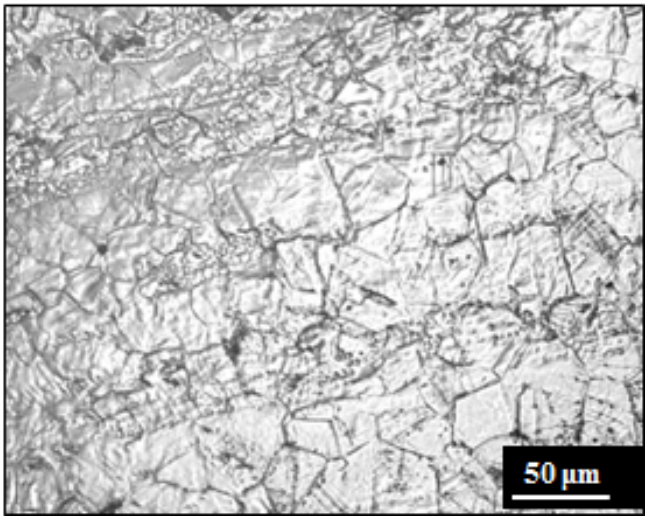

(b)

Figure 1: Optical micrograph of: (a) the laser cladded surface region, and (b) the 304L substrate.

After 24 hours of exposure, a chromium oxide layer had formed on the surface of the exposed samples. However, the sample that was laser cladded with stainless steel powder with 0wt% Ru had a defective oxide layer. Figure 2 (a) and (b) show the white patches which are the defects in the oxide layer at low and high magnifications at the highlighted areas respectively.

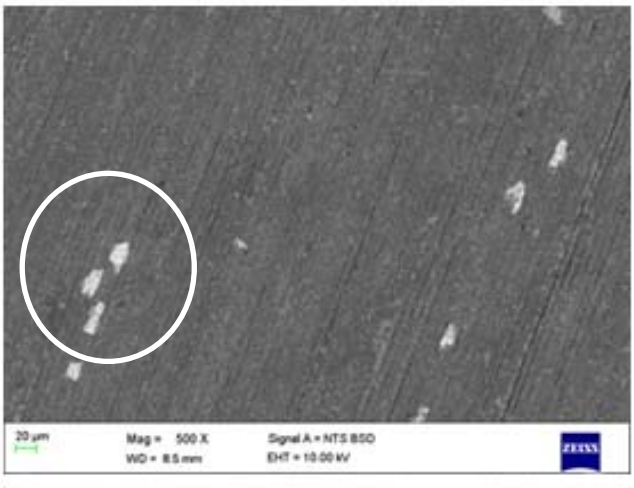

(a)

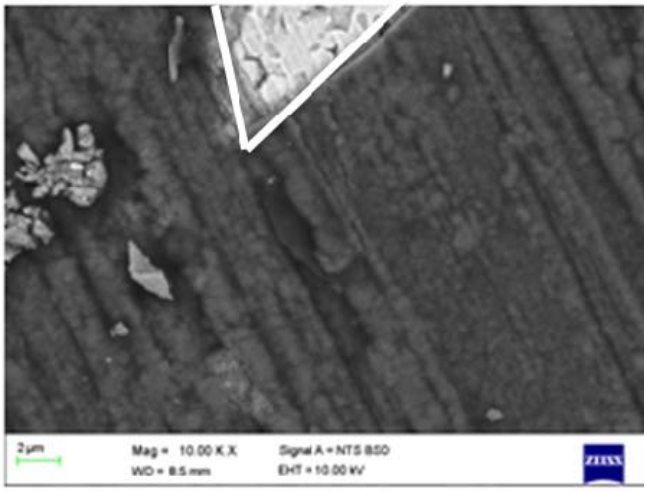

(b)

Figure2: SEM-backscattered image showing, defects in the oxide layer on the surface of the sample without Ru at (a) low magnification and (b) high magnification.

Deposited carbon was also observed on the surface, which was confirmed by EDS. The samples that were cladded with ruthenium did not show any defects in the oxide layer observed on the surface, Figure 3. After an additional 72 hours of exposure, the surface analyses of the 0wt%, 0.5wt% and 2wt% ruthenium samples showed islands of oxides that had formed on the continuous oxide layer. Figure 4 (a), (c) and (d) show the islands analysed with EDS, which showed that they were (Fe, Cr, Ni, Mn)oxide with minor traces of carbon which were detected as well. The islands appear to decrease in quantity as the ruthenium content is increased.

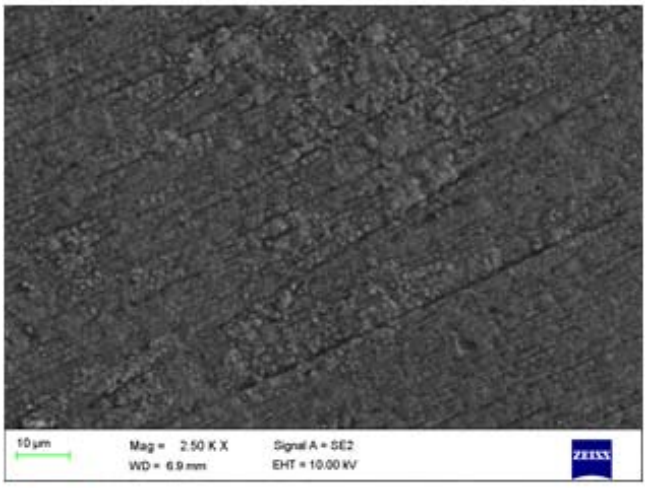

(a)

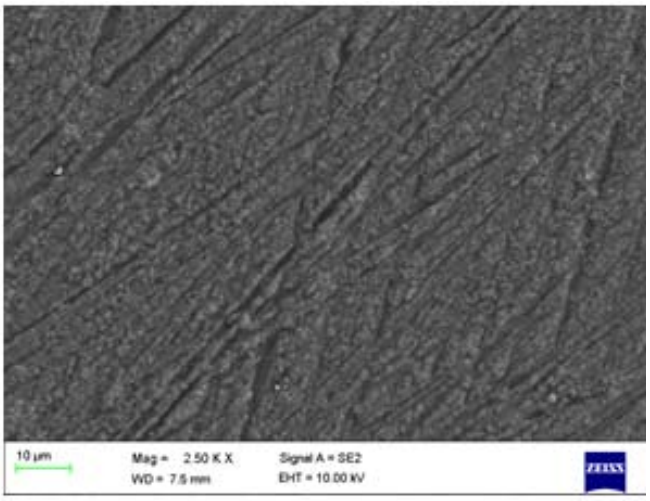

(b)

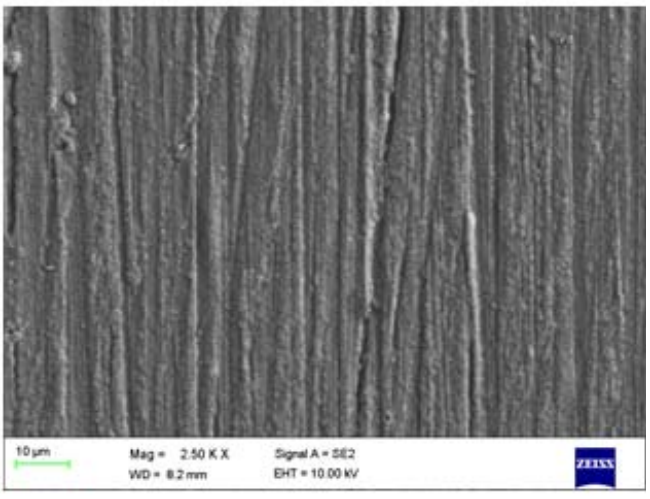

(c)

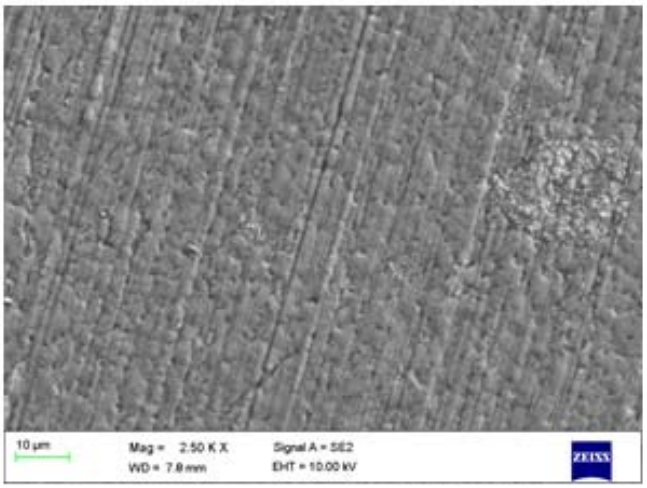

(d)

Figure 3: SEM-SE images showing the surface morphology of the exposed samples after 24 hours with no defects in the chromium oxide layer; (a) 0.5wt% Ru, (b) 2wt% Ru, (c) 5wt% Ru and (d) 10wt% Ru

In addition to the islands, the sample without ruthenium had a defective oxide layer, Figure 4 (b); this was not observed on any of the other samples**.** The Raman spectroscopy results showed that the islands observed on the 0wt% Ru are made up of hematite, where the 0.5wt% Ru which was identified to be manganese oxide and both oxides contain amorphous carbon as shown in Figure 5 (de Faria et al. 1997; Haskin et al. 1997; Julien et al. 2003). The 2wt% Ru containing sample was identified by Raman Spectroscopy to contain $NiCr_2O_4$ oxide as well as disordered carbon which is slightly graphitic (Kim & Hwang 2005; Mi et al. 2005).

EDS and Raman spectroscopy analyses showed that the smooth, dark and flat surface morphology regions were identified to be amorphous carbon mixed with (Cr, Ni, Fe, Mn) spinel oxides. In previous studies spinel oxides were often found covering the protective chromium oxide layer, so it is suspected that underneath them sits the protective oxide layer (Grabke & Müller-Lorenz 1998; Grabke 2003). At higher magnification, a defect was observed in the oxide layer of the sample without ruthenium. This defect was analysed using EDS which showed that the region was an oxide layer, Figure 4 (b) and is indicative of the substrate's re-healing abilities. The EDS results showed that the oxide is an (Fe, Mn, Cr)

oxide. The samples with the higher ruthenium contents showed a continuous oxide layer on the surface with regions of deposited carbon.

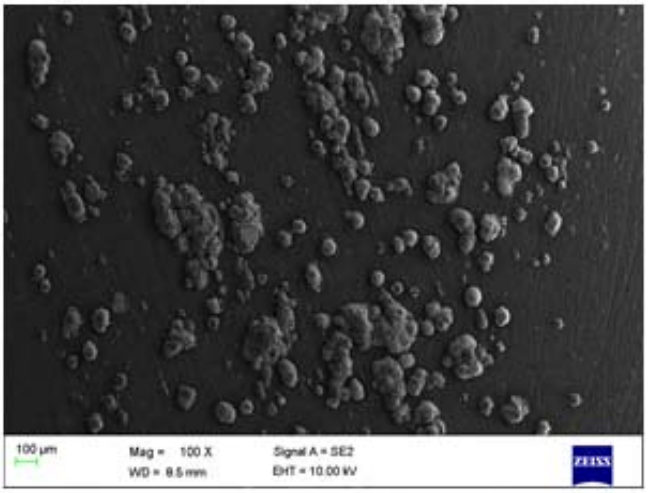

(a)

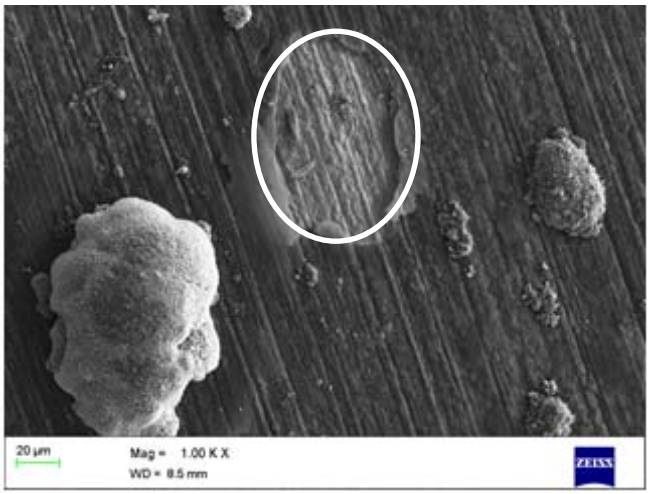

(b)

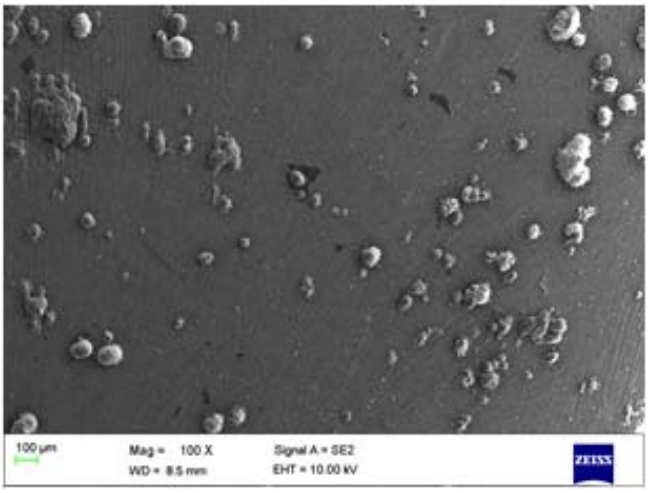

(c)

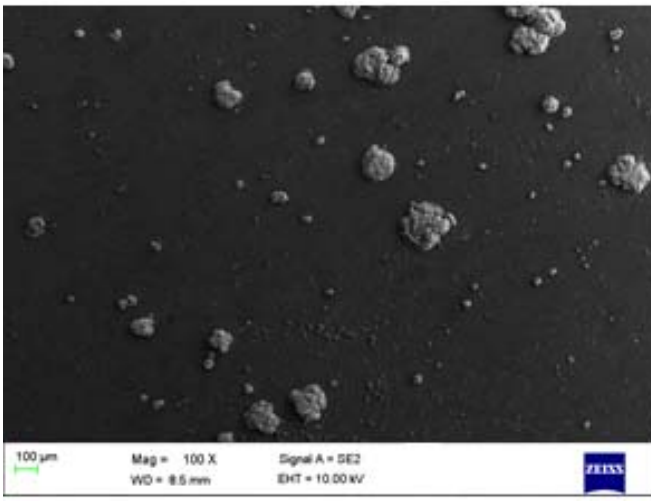

(d)

Figure 4: SEM-SE image showing the surface morphology with, oxide islands of (a) 0wt%Ru (b) 0wt% Ru at higher magnification and the circled self-healing defective oxide layer, (c) 0.5wt% Ru and at (d) 2wt%Ru.

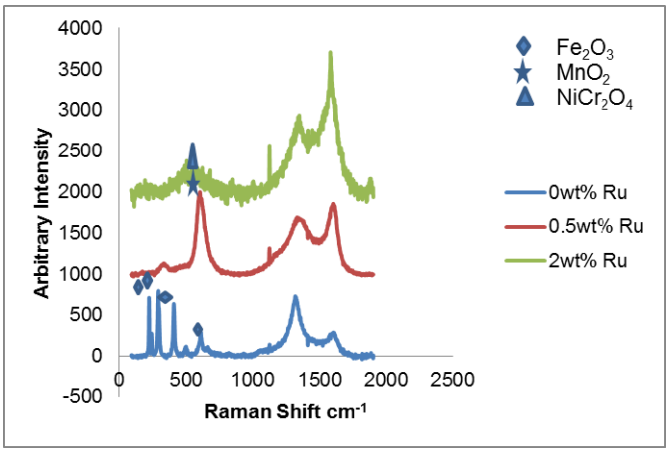

Figure 5: Raman spectra of the islands formed on the samples.

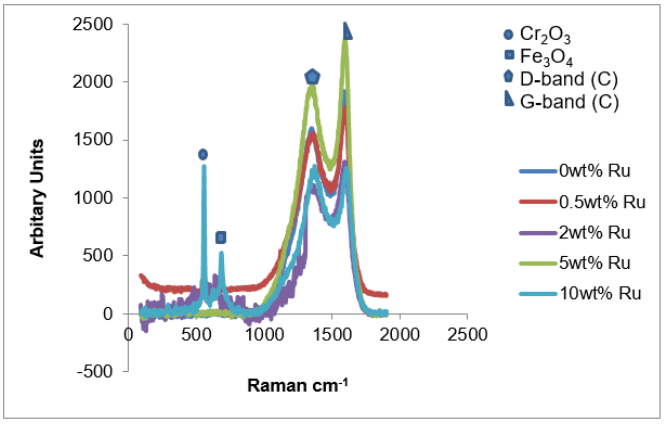

Figure 6: Raman Spectra for the smooth surfaces on the samples after exposure.

The Raman analysis results of the 5 and 10wt% ruthenium samples showed disordered carbon. Traces of magnetite and the chromium oxide were found on the surface of the 10wt% ruthenium, as well as carbon, Figure 6 (Kim and Hwang 2005).

The SEM surface morphology analysis done on the sample with 5wt% Ru, had regions with higher ruthenium concentrations and a dark layer that was flaking off which was determined to be predominantly carbon as circled in Figure 7 (a). Figure 7 (b) shows the 10wt% ruthenium sample which showed a homogeneous oxide layer mixed with ruthenium and no sites of ruthenium enrichment were observed. The oxide layer was also covered in the black carbon deposit which was flaking off. The results of the cross-section show that all the materials, apart from the 10wt% Ru coating, experienced shallow internal cracking.

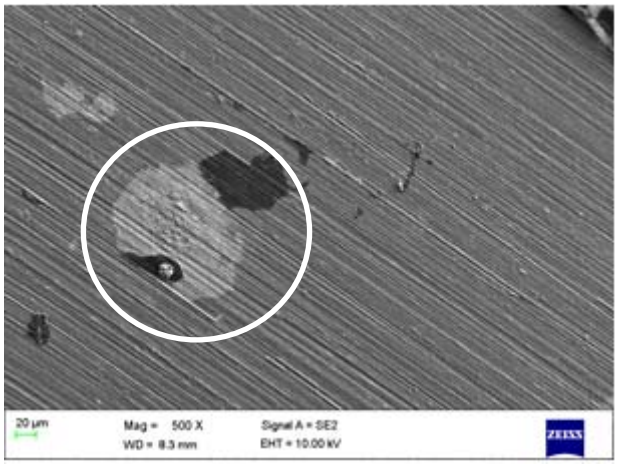

(a)

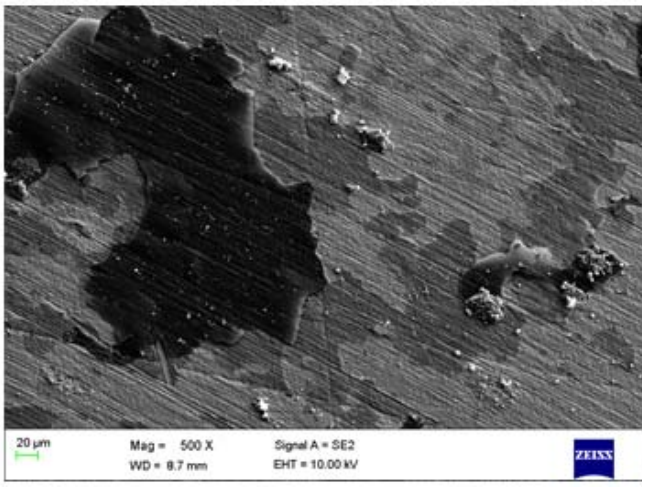

(b)

Figure 7: SEM-SE showing the surface morphology of: (a) 5wt% Ru with oxide layer and pronounced ruthenium islands, and (b) 10wt% Ru with an oxide layer mixed with ruthenium which is homogeneous and islands of carbon.

The sample without Ru exhibited cracking and oxide formation near the surface of the cross section. EDS analysis was performed on the phase close to the cracks in the circled region of Figure 8 (a), identifying the components that made up the substrate and oxygen. No carbon was detected in the cracks or the oxide formed internally. The 0.5wt% Ru sample did not exhibit many cracks, and they were identified at very high magnifications and began directly underneath the oxide scale where it healed itself, figure 8 (b). The internal oxides and cracks are suspected to have originated from sites where the oxide layer had broken up but healed itself and this healing was accompanied by the islands identified in Figure 4. The cross-section of the 10wt% Ru sample did not have any subsurface cracks. As ruthenium was increased on the alloy surface the protection against attack was improved.

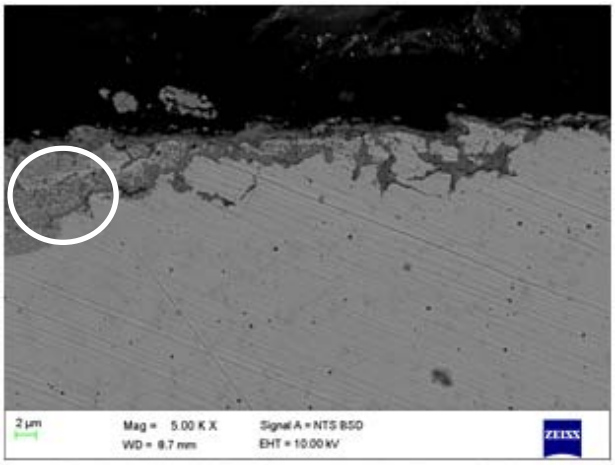

(a)

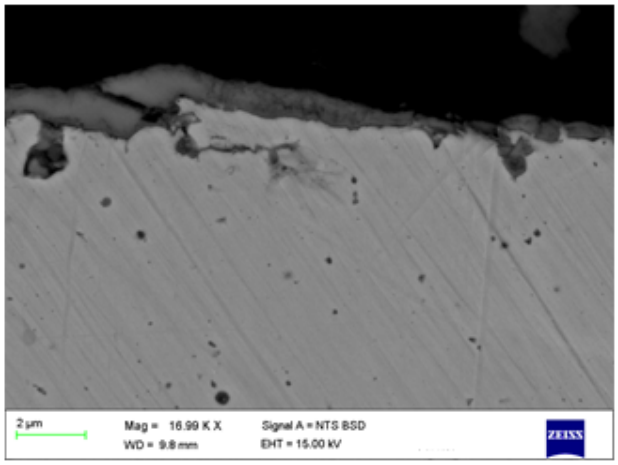

(b)

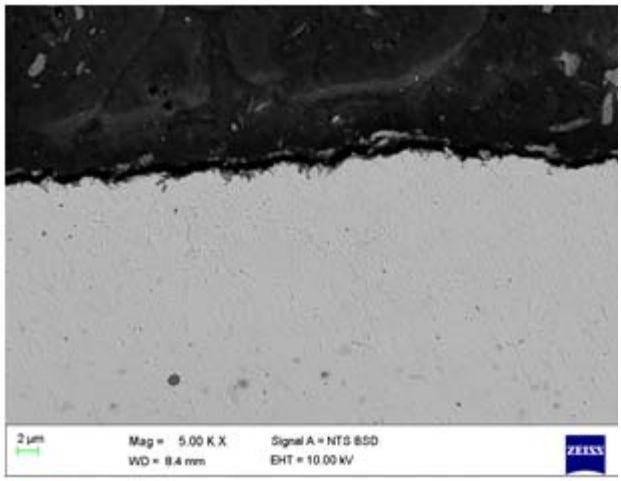

(c)

Figure 8: SEM-backscattered images of cross-sections of, (a) 0wt% Ru, (b) 0.5wt% Ru, and (c) 10wt% Ru

4 Discussion

The formation of the chromium oxide layer is generally enhanced by the presence of smaller grains which result in a larger grain boundary surface area, and grinding which increases the density of dislocations. Both these material features improve the diffusion of chromium because they increase diffusion paths (Leistikow & Grabke 1987; Grabke & Müller-Lorenz 1998; Grabke 2000). The formation of the oxide layer was greatly enhanced by the laser cladding and ruthenium additions, which resulted in a refined microstructure, Figure 1 (a), which resulted in a high density of grain boundaries that allowed for easy chromium diffusion. Another contributing factor to the enhancement of the formation and growth of the oxide layer was the operating temperature; Grabke stated that temperatures of 700°C and above allowed chromium to segregate to the surface much faster (Grabke & Wolf 1987; Grabke & Müller-Lorenz 1998; Grabke 2000). A high temperature and low PO_2 results in the formation of a continuous oxide layer, which would be the case in this work, because the source of oxygen was 2ppm, present as an impurity in the nitrogen carrier gas (Grabke & Wolf 1987; Grabke & Müller-Lorenz 1998; Grabke 2000). It was no surprise that the oxide layer was able to re-heal itself because the temperature at which the exposure was conducted as well as the refined microstructure allowed for easy chromium diffusion, Figure 4 (b). The addition of ruthenium maintained a continuous and protective oxide layer which was free of defects by improving chromium diffusion to the surface as well; Figure 4 (c) and (d) and Figure 7. Previous studies showed (van Staden & Roux 1990a; van Staden & Roux 1990b) that the additions of ruthenium to Fe-Ni-Cr alloys depress the migration of iron to the surface and promote that of chromium. The constant supply of chromium to the surface contributes to the formation and the self-healing ability of the oxide layer, and so does the presence of ruthenium (van Staden & Roux 1990a; van Staden & Roux 1990b; Tjong & Shih 1991; Wolff et al. 1998). The oxide layer has been shown to slow down metal dusting (Wiemer et al. 1991, Grabke & Müller-Lorenz 1998); from the results obtained it is evident that the oxide layer does slow down the onset and occurrence of metal dusting because no pitting which is evidence of metal dusting was observed on any of the samples tested.

The islands that formed on the surface of the material are suspected to be due to differential diffusion, which was promoted by the defects in the oxide layer exposing the substrate which contained a low concentration of alloying elements of 304L. These alloying elements therefore diffused outwards to the surface in order to equilibrate the surface composition. The diffusion of Fe, Mn, Ni to the surface of the substrate allows for formation of a spinel oxide on the surface covering a bottom layer of the protective chromium oxide layer. Cracks observed in the cross-section have been found in other works to be a result of the formation of internal carbides, or internal oxidation or volume

expansion due to graphitization within the material (Szákalos et al. 2002a; Hänsel et al. 2003; Szákalos 2003). However, in the current study no carbides and graphite were identified in the cracks, only oxygen was detected near and around the cracks. It appears that the oxide layer grew inwards into the material because the cracks follow an intergranular path indicating that the oxygen diffused inwards along the grain boundaries and such a phenomenon has been reported to be a subsurface form of attack which is termed internal oxidation (Chatterjee et al. 2001; Young & Gleeson 2002; Hänsel et al. 2003). Internal oxidation occurs as a result of the oxygen from the atmosphere diffusing much quicker than the alloying elements in the substrate to form an external oxide layer, therefore resulting in the formation of the internal oxide layer first. Thereafter the external oxide formed when a high concentration of oxide forming alloying elements had been achieved the external protective layer. This phenomenon often occurs along the grain boundaries, as opposed to the grains, hence the intergranular type attack that has been observed on the cross-sections of the samples (Chatterjee et al. 2001; Szákalos et al. 2002b; Hänsel et al. 2003). It has been reported that the lack of carbon in these internal oxides maybe a result of sufficient oxygen dissolving into the material to a point that it oxidised the internal carbides precipitated in the substrate and oxidised the substrate, hence it was not found in the EDS analysis (Lin et al. 2004).

Another observation worth mentioning which appears to have propagated the internal oxidation is that the sites where the oxide layer had spalled, may have also been sites of entry for the oxygen to form the internal oxides observed, especially in the 0wt%-2wt% Ru samples. The 5 and 10wt% Ru samples were the two best performing alloys because as ruthenium content increases so does the formation and self-healing effect of the chromium protective layer therefore minimizing metal dusting.

5 Conclusion

At 750ºC, the laser cladded surface alloys formed a protective and continuous oxide layer which was attacked at 24 hours for the sample laser cladded with stainless steel powder, although the observed defects were able to self-heal. The 5 and 10wt% Ru samples formed continuous and adherent protective oxide layers, which protected the 304L substrate against metal dusting. Laser cladding and the addition of ruthenium at 750ºC results in an increased metal dusting incubation period and the samples are able to self-heal over a period of 96 hours. No metal dusting was observed over this period.

Acknowledgements

We would like to thank the DST-NRF Centre of Excellence in Strong Materials for providing the funding for this project as well as the Corrosion Institute of Southern Africa for their partial funding in the form of the Ivan Oglivie award. We would also like to acknowledge Doctor Rudolph Erasmus for his assistance with the Raman Spectroscopy analysis and help with interpreting the results, Ndivhuwo Nelwalani for his assistance with the SEM analysis. And lastly the university workshop staff for their help with the cutting and sectioning of samples and lastly Shahil Ramallal for his assistance with setting up the experimental rig.

References

Agüero, Gutiérrez, M., Korcakova, L., Nguyen, T.T.M., Hinnemann, B. & Saadi, S., 2011. Metal dusting protective coatings. A literature review. *Oxidation of Metals*, 76(1-2), pp.23–42.

Chatterjee, U.K., Bose, S.K. & Roy, S.K., 2001. Environmental degradation of metals: Corrosion Technology Series/14, First., Marcel Dekker.

Chun, C.M. & Ramanarayanan, T. A., 2007. Corrosion resistance of a high-silicon alloy in metal-dusting environments. *Oxidation of Metals*, 67(3-4), pp.215–234.

de Faria, D.L. A., Silva, S.V. & de Oliveira, M.T., 1997. Raman microspectroscopy of some iron oxides and oxyhydroxides. *Journal of Raman Spectroscopy*, 28, pp.873–878.

Geers, C., Galetz, M. & Schütze, M., 2013. Investigation of the effect of the alloy 600 substrate for the stability of a Ni_3Sn_2 coating for metal dusting protection at 620°C. *Surface and Coatings Technology,* 215, pp.2–6.

Grabke, H. & Wolf, I., 1987. Carburization and oxidation. *Materials Science and Engineering*, 87, pp.23–33.

Grabke, H.J. & Müller-Lorenz, E.M., 1998. Protection of high alloy steels against metal dusting by oxide scales. *Materials and Corrosion*, 49, pp.317–320.

Grabke, H.J., 2000. Surface and interface phenomena in oxidation of alloys. *Electrochemical Society Proceedings: Kofstad Memorial Symposium-High Temperature Corrosion and Materials Chemistry*, pp. 60–67.

Grabke, H.J., 2003. Metal Dusting. *Materials and Corrosion*, 54(10), pp.736–746.

Grabke, H.J., Martinz, H.P. & Müller-Lorenz, E.M., 2003. Metal dusting resistance of high chromium alloys. *Materials and Corrosion*, 54(11), 860–863.

Hänsel, M., Boddington, C. A. & Young, D.J., 2003. Internal oxidation and carburisation of heat-resistant alloys. *Corrosion Science*, 45(5), pp.967–981.

Haskin, L.A., Wang, A. & Jolliff, B.L.P., 1997. Raman spectra of birnessite manganese dioxides. *Solid State Ionics*, 159(3-4), pp.345–356.

Kim, J.H. & Hwang, I.S., 2005. Development of an in situ Raman spectroscopic system for surface oxide films on metals and alloys in high temperature water. *Nuclear Engineering and Design*, 235(16), pp.1773.

Leistikow, S. & Grabke, H.J., 1987. Effects of cold work on the oxidation behavior and carburization resistance., *Materials and Corrosion*, 101 (38), pp.556–562.

Lekala, M.B., Van Der Merwe, J.W. & Pityana, S.L., 2012. Laser surface alloying of 316l stainless steel with Ru and Ni mixtures. *International Journal of Corrosion*, pp.1–5.

Lin, C.Y., Chang, C.H. & Tsai, W.T., 2004. Morphological and microstructural aspects of metal dusting on 304L stainless steel with different surface treatments. *Oxidation of Metals*, 62(3-4), pp.153–174.

Melo-Máximo, L. et al., 2013. Performance of Cr oxide coatings on 304 steel against metal dusting. *Surface and Coatings Technology*. 237, pp.39-50.

Mi, Y., Yuan, D., Zhang, J. & Xiao, Y., 2005. Synthesis of carbon nanotubes via toluene-thermal reduction process at moderate temperature. *Journal of Materials Science*, 40, pp.3635–3638.

Olubambi, P.A., Potgieter, J.H. & Cornish, L., 2009. Corrosion behaviour of superferritic stainless steels cathodically modified with minor additions of ruthenium in sulphuric and hydrochloric acids. *Materials and Design*, 30(5), pp.1451–1457.

Palasantzas, G., Kooij, H.J. & DeHosson, J.T.M., 2004. Carbon induced metal dusting of iron-nickel-chromium alloy surfaces: A scanning auger microscopy study. *Applied Surface Science*, 229(1-4), pp.190–196.

Rowlands, D.P. (2006). Stainless steel: an introduction to an exciting and versatile material, classification, typical properties and applications the family of stainless steel the corrosion resistance of stainless steel, *Southern Africa Stainless Steel Development Association*, (1), 1-6.

van Staden, M.J & Roux, J., 1990a. Surface Segregation in the Alloys Fe-40Cr-3Ru, Fe-40Cr-3Pt and Fe-40Cr with a 1000 Å Pt. Applied Surface Science, 44, pp.271–277.

van Staden, M.J & Roux, J., 1990b. The controlled oxidation of the high chromium steel alloys Fe40Cr and Fe40Cr3Ru. *Applied Surface Science*, 44, pp.263–269.

Strauß, S., Krajak, R. & Grabke, H.J., 1999. Coking by metal dusting of nickel-base alloys. *Materials and Corrosion*, 50(11), pp.622–627.

Szakalos, P., Pettersson, R. & Hertzman, S., 2002a. An active corrosion mechanism for metal dusting on 304L stainless steel. *Corrosion Science*, 44, pp.2253–2270.

Szakalos, P., Pettersson, R. & Hertzman, S., 2002b. Carburization, carbide formation, metal dusting, coking. *Materials and Corrosion*, 46(5), pp.1890–1896.

Szakálos, P., 2003. Mechanisms and driving forces of metal dusting. *Materials and Corrosion*, 54(10), pp.752–762.

Szakálos, P., 2004. Mechanisms of metal dusting. PhD Thesis, Royal Institute of Technology, Stockholm, Sweden.

Tjong, S.C. & Shih, C.Y., 1991. Oxidation characteristics of some Fe-40Cr-Pd and Fe-40Cr-Ru alloys in air at 900 ° C. *Journal of Material Science*, 27, 1818-1826.

Wiemer, D., Grabke, H.J. & Viefhaus, H., 1991. Investigation on the influence of sulfur segregation on the adherence of protective oxide layers on high temperature materials. *Fresenius' Journal of Analytical Chemistry*, 341(5-6), pp.402–405.

Wolff, I.. et al., 1998. Oxidation and corrosion behaviour of Fe–Cr and Fe–Cr–Al alloys with minor alloying additions. *Materials Science and Engineering*: A, 241(1-2), pp.264–276.

Young, D.J. & Gleeson, B., 2002. Alloy phase transformations driven by high temperature corrosion processes. *Corrosion Science*, 44(2), pp.345–357.

Zeng, Z. & Natesan, K., 2006. Initiation of metal-dusting pits and a method to mitigate metal-dusting corrosion. *Oxidation of Metals*, 66(1-2), pp.1–20.

Zeng, Z., Natesan, K. & Maroni, V. A., 2002. Investigation of metal-dusting mechanism in Fe-base alloys using Raman spectroscopy, X-ray diffraction, and electron microscopy. *Oxidation of Metals*, 58(1-2), pp.147–170.

Zhang, J. & Young, D.J., 2007. Effect of copper on metal dusting of austenitic stainless steels. *Corrosion Science*, 49(3), pp.1450–1467.

Zhang, J., Speck, P. & Young, D.J., 2012. Metal dusting of alumina-forming creep-resistant austenitic stainless steels. *Oxidation of Metals*, 77(3-4), pp.167–187.